American Journal of
Nanoscience and Nanotechnology Research
http://www.ivyunion.org/index.php/ajnnr

Research Article

The Role of Solvents' Dielectric Constants in the Delicate Interplay between Microstructure and Optical Properties of Poly (3-Hexylthiophene) Thin Films

Agumba O. John*

Department of Physics, School of Pure and Applied Sciences (SPAS),
Pwani University, Kilifi, KENYA

Abstract:
In order to gain a deeper understanding of the interplay between microstructure and functional properties of conducting polymers such as their optical behaviors, precise control of the structure formation methods of such polymers is of great importance. This work concerns the study of the role of solvents on the formation of different structures and how the resultant structural features affect the functional optical properties of a model Poly (3-hexylthiophene) conjugated system. Thin films of P3HT have been formed from solvents of different polarities and the structural features of the resultant films studied using optical microscopy and XRD technique. The photo-physical characteristics have been studied using UV-Vis spectroscopy and photoluminescence (PL) spectroscopy. We report that the nature of polymer structure and thus the resultant optical properties greatly depend on the solvent polarity and their dielectric constants rather than their solubility power. We have asserted that the solvent polarities have their fingerprints in the resultant film crystallinities, grain sizes, optical photoluminescence and the optical band gaps and by extension on the opto-electronic device applications.

Keywords: Poly (3-hexylthiophene); Optical Band Gap; Absorbance; Photoluminescence; Polarity; Dielectric Constant
Received: November 22, 2018; **Accepted**: December 21, 2018; P**ublished**: January 25, 2019
Competing Interests: The author has declared that no competing interests exist.

***Correspondence to**: Agumba O. John, P.O. Box 195-80108, Kilifi, Kenya
Email: agumba.john@gmail.com

1. Introduction

Poly(3-alkylthiophenes) are special class of polymers with good solubility in most organic solvents, eas processability, high crystallinity, high light absorbability, good hole transport, excellent thermal stability, good environmental stability and optical band gap in the range of 1.7–2.1 eV [1, 2]. These features make them the most widely used conjugated polymers for organic optoelectronic applications in devices such as OLED, OFETs and organic solar cells. The two main structural characteristics of electronically or optically active polymer design are a conjugated backbone for photon absorption and side chain substitution for their solubility [3, 4]. However, reliable control of the material performance in these functional structures has remained challenging due to the random nature of molecular conformations, packing, and morphologies. The choice of processing techniques control the degree of crystallinity as well as the sizes of these crystalline regions and by extension, the bulk material performance [5, 6]. Factors such as the polymer molecular weight, the solvent used and generally the self assembly process can be used to study this interplay. In solution, polymer chains can experience diverse chain conformation ranging from swollen to highly aggregated states depending on the relative strength of the polymer–solvent (P–S) and polymer–polymer (P–P) interaction [7–11]. In 'good' solvents, the P–S interaction dominates over P–P interactions and the polymer chains are completely dissolved and have a swollen conformation. Necessary to mention, there is increase of the radius of gyration, R_g, for ''better'' solvents (Higher Flory-Huggins parameters).This means that during crystal formation (aggregation), the chain conformation is more relaxed in better solvents. Loosening the chain conformation would allow polymer chains to uncoil and find the lowest energy position in a crystal more easily, decreasing the likelihood of forming defects. Hence a more defect free structures are expected to form in better solvents than in poor ones. On the other hand, the P–P interactions dominate in 'poor' solvents and the polymer chains aggregate and form compact objects like three dimensional (3D) globules, two-dimensional (2D) discoids [9] or one-dimensional (1D) rod-like particles (cylinders) [7, 9- 11, 13]. In the middle between the good and the bad solvents are the are θ-solvents, where the P–S and P–P interactions are balanced and the polymer chains tend to assume random-coil conformations similar to the Gaussian coil of an ideal polymer chain[12]. The type of the solvent used thus determines the polymer chain ordering that may be dominated by either interchain or intrachain interaction of the monomer units within the chain segments.

Spano and coworkers have used the absorbance peak intensity ratios ($A_{0\text{-}0}/A_{0\text{-}1}$) to test the degree of crystalline quality in P3HT aggregates [14]. When intrachain order (i.e., planarity of monomers within chain segments) is low, optical spectra resemble H-aggregates where the electronic origin (0−0) transition is less intense than the 0−1 vibronic sideband. Larger $A_{0\text{-}0}/A_{0\text{-}1}$ ratios indicate increased intrachain order and smaller values are indicative of an increase in interchain order. For H-aggregates, the ratio is less than unity (<1) and is inversely proportional to the excitonic bandwidth (W). The opposite trends are expected for J-aggregates which are very rare for P3HT. In fact, the weakly coupled H-aggregate model of Spano has been successfully used to deconvolute the contributions from aggregates as well as to estimate the coupling strength and intrachain order within aggregates [14]. We have investigated the role of solvent polarities and thus dielectric constant on the crystallization behavior of P3HT and the effect on the photo-physical properties of the resultant polymer films.

2. Materials and Methods

2.1 Equipment

Regioregular poly(3-Hexylthiophene) (P3HT) of M_n ~ 64000 g/mol, regioregularity of 98% was purchased from Sigma Aldrich and was used as received without further purification. X-Ray Diffraction was performed using multi-purpose X-ray diffractometer (Philips X'Pert MPD system). The CuKα radiation was used (λ = 1.54 A°). The data were collected at room temperature in the 2θ range. The UV/Vis absorption spectra were collected using an Agilent Cary 5000 UV-Vis-NIR spectrometer equipped with an integrating sphere in the wavelength range of 300-800 nm. A Horiba Fluorolog-3 FL3-122 with a Xenon 450 W excitation source was used for PL measurements.

2.2 Sample Preparation

Four samples were prepared for investigation. A solution of P3HT in 3-Hexylthiophene (3-HT) solvent of concentration 0.20mg/ml was prepared at 90 ^{o}C. Uniformly orange solution was formed after heating for 5 minutes. For sample A, 0.2 mg/ml of P3HT in THF was prepared at 60 ℃ in an oil bath until homogenous light orange solution was formed. The solution was then quickly transferred to another thermostat kept at 5 ℃ and left for isothermal crystallization for 24 hrs. For sample B, 0.2 mg/ml of P3HT was prepared in $CHCl_3$ at 50 ℃ in an oil bath until homogenous light orange solution was formed. The solution was then quickly transferred to another thermostat kept at 2 ℃ and left for isothermal crystallization for 24 hrs. For sample C, 0.2 mg/ml of the solution was prepared in Toluene at 70 ℃ in an oil bath until homogenous light orange solution was formed. The solution was then quickly transferred to another thermostat kept at 10 ℃ and left for isothermal crystallization for 24 hrs. Figure 1 shows vials containing the solutions for the different samples. After the isothermal crystallization of the three solutions, 100 µl of each were drop cast on 1.0 cm by 1.0 cm cleaned silicon substrates and the solvents left to evaporate at ambient conditions. Optical microscopy was then performed using optical Motic microscope on these samples to observe any structure formed.

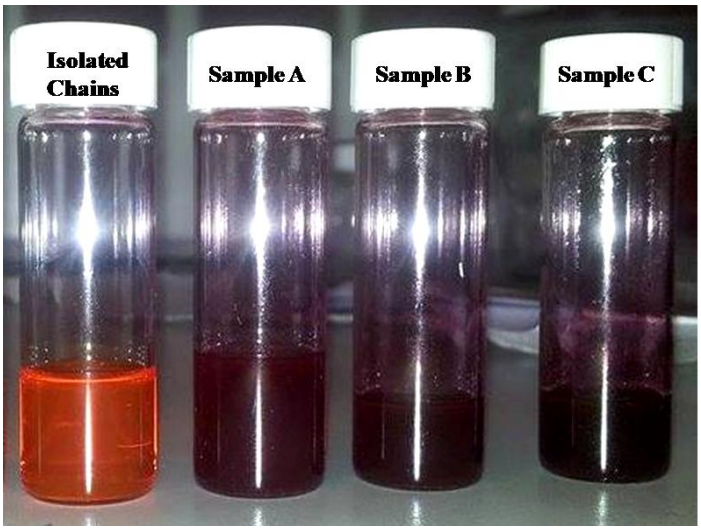

Figure 1 Photographs of a fully dissolved P3HT solution prepared in 3-HT, aggregated solutions prepared from THF (sample A), $CHCl_3$ (sample B) and Toluene (sample C).

3. Results and Discussions

3.1 Structural Characterization

3.1.1 Optical Microscopy

The diagram below shows a fully dissolved P3HT solution prepared in 3-HT in a 10.0 mm cuvette and optical micrographs of thin films of sample A, sample B and sample C.

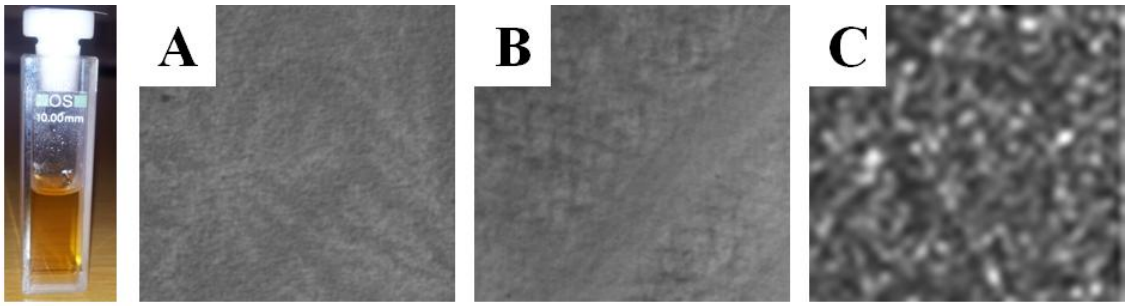

Figure 2 Diagram showing a fully dissolved P3HT solution in a 10.0 mm cuvette prepared from 3-HT and thin films of P3HT solutions prepared from THF (sample A), $CHCl_3$ (sample B) and Toluene (sample C). (The micrograph sizes are 250 μm by 250 μm)

The micrograph from samples A shows a number of non-uniformly distributed structures while the micrograph from sample B shows clustered structures. The micrograph from sample C shows well-defined nanocrystals which could be composed of extended chains. These different structures could be due to the fact that toluene is a marginal solvent while THF and $CHCl_3$ (solubility ≈ 14 mg/mL), [15]) are better solvents for P3HT. The polymer chains are expected to have a higher degree of chain mobility and conformational freedom in the good solvents (samples A and B). The growth of 1D nanocrystals for sample C is driven by strong π–π-interactions and unfavorable interactions between the solvent and polymer backbone under limited solubility.

3.1.2 Wide Angle X-Ray Diffraction (WAXRD)

We performed temperature dependent WAXRD measurements to observe how the crystal structure of the P3HT thin films depended on the structure formation method (solvent). The Bragg reflections below were obtained for the three samples A, B and C.

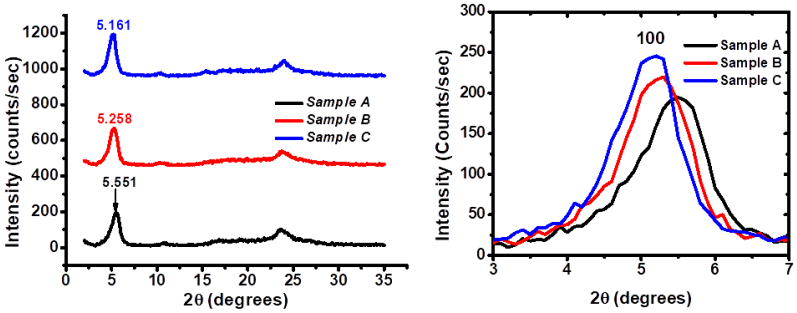

Figure 3 Wide-angle X-ray diffraction pattern of nanostructured P3HT films deposited on silicon. The diffractograms shows strongly enhanced 100 reflections Bragg peak yielding a form 1 monoclinic crystal structure. The 100 Bragg peak increases intensity from sample A to C with reduced full wave at half maximum (FWHM)

From the figure, the samples have peaks at $2\theta \sim 5.4318^{o}$, 5.2051^{o} and 5.0889^{o} for samples A, B and C corresponding to d_{100}-spacings, attributed to inter-chain lamella peaks .These peaks are possibly related to crystalline orientations of the thiophene units with respect to the substrate, which is similar with the literature reports [16, 17]. From the 100 diffraction peaks, the d-spacing (d_{100}) were calculated by employing the Braggs equation below and found to be 1.625 nm, 1.696 nm and 1.735 nm as depicted in the graph in Figure 4 (a).

$$n\lambda = 2d_{hkl}\sin\theta \quad \text{.....(1)}$$

The figure shows that the d-spacing increases with decreasing solvent polarities. Normally, the particle size (grain size) can also be calculated using the Debye-Scherrer equation (2).

$$D = \frac{\lambda k}{\beta \cos\theta} \quad \text{.....(2)}$$

Where λ=15.4 nm, $\theta = \frac{2\theta}{2}$ (scattering angle) and β is the FWHM of the peaks in radians.

We have calculated the grain size using equation (3);

$$D = \frac{0.9\lambda}{\beta \cos\theta} \quad \text{.....(3)}$$

We have taken $k=0.9$

Now $$D = \frac{51.55\lambda}{\theta \cos\theta} \quad \text{..... (4)}$$

where, the FWHM, β has been expressed in radians i.e. $\beta = \frac{22\theta}{7X180}$

Figure 4 (b) shows a graph of the particle (grain sizes for the three samples A, B and C as calculated from the Debye-Scherrer equation as discussed above. It is clear from the graph that the grain sizes increases with decreases in solvent polarities.

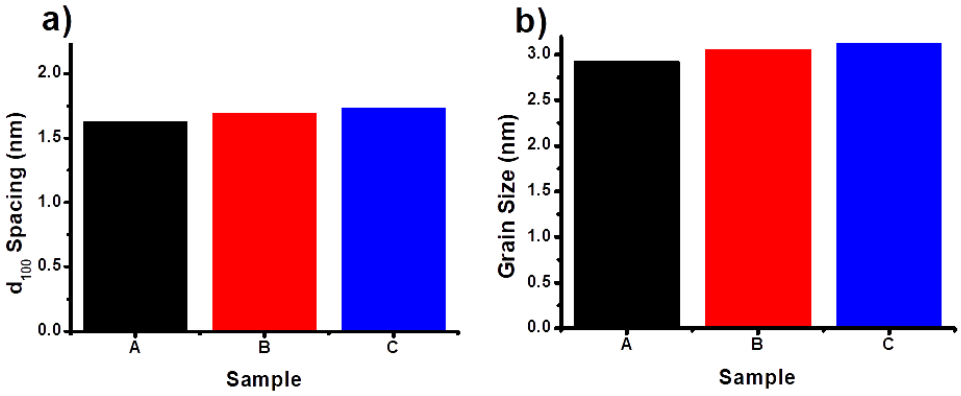

Figure 4 Graphs representing the d100 spacing and the grain size for the three samples A, B and C

Figure 5 (a) shows a graph representing the integrated intensities and the FWHM for the three samples A, B and C. Figure 5 (b) shows the dependence of the integrated intensities and FWHM on the solvent polarities (dielectric constants).

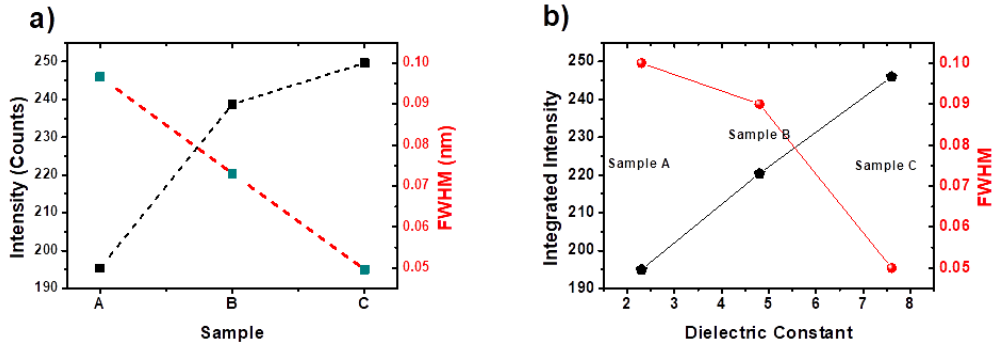

Figure 5 A graph of the integrated intensity for samples A, B and C (b). Graph (b) shows the integrated intensities and FWHM as functions of dielectric constants for the three samples A, B and C

From the graphs, the crystalline grain sizes and the integrated intensities increased with increasing solvent polarities (dielectric constants). The results show that the P3HT films are made up of many nano-crystallines and disorderly regions. From the data, the mean size of nano-crystalline region (FWHM) were found to decrease with increase in solvent polarities (increase in dielectric constants). However, the degrees of the film crystallinities (the integral intensity) were found to be directly proportional to the solvents' polarities [17].

3.2 Optical Characterization

3.2.1 Absorption Spectroscopy

The spectra in Figure 6 were recorded for the fully dissolved chains in solution and the three samples A, B, C prepared from different solvents.

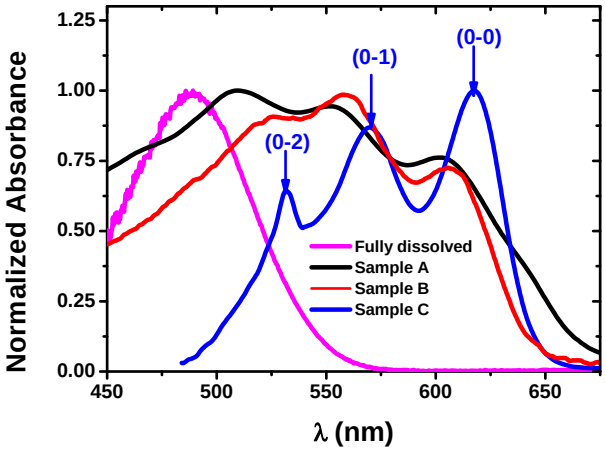

Figure 6 The typical absorption spectra from isolated chains P3HT 3-HT, thin films prepared from THF (sample A), in CH Cl_3 (Sample B) and in toluene (sample C). The vibronic features of the P3HT aggregates and fibers are labeled according to the number of vibrational quanta in the excited state

The UV-visible spectrum of the P3HT solution showed a single peak at λ= ~520 nm without structural features, which is associated with isolated chains in a coiled conformation [18]. According to Zen and coworkers, both repulsive interactions between successive monomer units and interactions between the solvent and the side chains drive a dihedral twist of the polymer backbone in solution [19]. Sample A showed two peaks at λ=~508 nm and ~553 nm and one shoulder peak at λ=~602 nm. Sample B showed two peaks at λ= ~520 and ~560 nm and one shoulder at λ= ~607 nm. Sample C showed two peaks at λ= ~531 nm and ~562 nm and one shoulder at λ= 618 nm. The three bands for samples A, B and C are also called vibronic absorption shoulders. These three bands can be attributed to the π–π* transition in crystalline π-π stacking structure of polymer P3HT chains (conjugated polymer), [14, 20]. The higher the P3HT order the more inter-digitation and stacking occurs, the more pronounced are the vibronic shoulders. The crystallinity is manifested in absorption as a series of vibronic transitions labeled as *0-n* (n=*0, 1, 2,…)* where *n* is the number of vibrational quanta in the terminal excited state. The energy separation is usually taken as ~1450 cm^{-1} (170 meV) corresponding to symmetric vinyl stretch. It is important to note that, the Spano model assumes that the magnitude of exciton coupling is smaller than the frequency of the dominant displaced phonon vibration in P3HT (i.e., C=C mode usually taken as ca. 180 meV) [14, 20]. By considering a weak-coupling limit where we consider only nearest neighbors coupling as suggested by Spano, we have estimated the excitonic coupling constant, j_0 from the relative absorption strengths ($A_{0\text{-}0}/A_{0\text{-}1}$) of the 0-0 and 0-1 transitions from equation 5 [14-22].

$$j_0 = \left[\frac{E_p\left(1-\sqrt{\frac{A_{0-0}}{A_{0-1}}}\right)}{0.48+0.146\sqrt{\frac{A_{0-0}}{A_{0-1}}}} \right] \quad \text{.....(5)}$$

where E_p is the energy (eV) of the vibrational transition coupled to the electronic transition, here taken to be 0.17 eV, and $A_{0\text{-}0}/A_{0\text{-}1}$ is the ratio of absorption intensities. Table 1 shows properties of the three samples.

Table 1 The summary of the dielectric constants, oscillator strength ratios $A_{0\text{-}0}/A_{0\text{-}1}$, the excitonic constant type, jo, the excitonic bandwidth, W and the aggregate type for the three samples A, B and C.

Sample	Dielectric Constants (ε)	$A_{0\text{-}0}/A_{0\text{-}1}$	Excitonic Coupling Constant j_0 (meV)	Excitonic Bandwidth W(meV)	Aggregate Type
A	7.6	0.985	+2.04	8.16	H
B	4.8	0.803	+28.9	115.6	H
C	2.3	1.133	-17.2	68.9	J

From Table 1, the $A_{0\text{-}0}/A_{0\text{-}1}$ ratio for sample A is ca. 0.9850 corresponding to numerical value of j_0=+2.04 meV. For sample B, $A_{0\text{-}0}/A_{0\text{-}1}$ ratio is ca. 0.80301 and corresponds to a numerical value of j_0=+28.9 meV. These two values of excitonic coupling constant, j_0 implies strong interchain exciton coupling a characteristic feature of a weakly coupled H-aggregate for the two structures. Interestingly, for sample C, $A_{0\text{-}0}/A_{0\text{-}1}$ ratio is ca. 1.133 corresponding to a numerical value of j_0=-17.23 meV implying strong intrachain exciton coupling which is a characteristic feature of a J-aggregate. The excitonic bandwidth parameter W has been calculated from the equation given by;

$$W = \left|4J_0\right| \quad \ldots\ldots (6)$$

For the H-aggregate like structures, the excitonic band widths W were found to be 8.2 meV and 115.6 meV for samples A and B respectively. For the J-aggregate like structure C, the excitonic band width, W was found to be 68.9 meV. These values are represented in Figure 7.

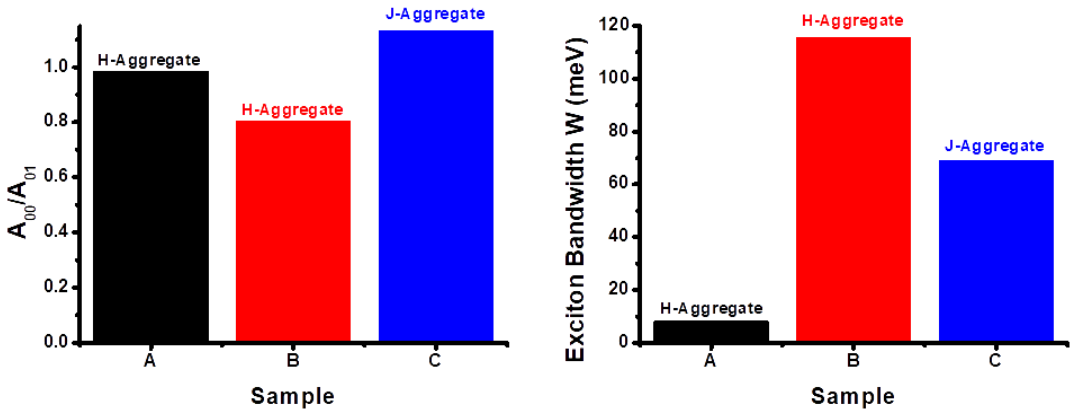

Figure 7 The absorption intensity ratios $A_{0\text{-}0}/A_{0\text{-}1}$ and the excitonic band widths for three samples A, B, C

The degree of coupling between chains manifests itself in the absorbance spectra as the ratio of the

lowest energy peak $A_{0\text{-}0}$ and the next replica peak $A_{0\text{-}1}$ heights. An increase in $A_{0\text{-}0}/A_{0\text{-}1}$ peak ratio as has been observed for the samples A, B and C corresponds to decrease in interchain excitonic coupling $J_{inter.}$, Intuitively, this leads to an increase in intrachain excitonic coupling J_{intra} resulting from increase in conjugation length and intrachain order. A negative excitonic coupling, J and the excitonic bandwidth, (W) suggests that the polymer chains within the crystals do not behave as H-aggregates but as J-aggregates. The excitonic coupling between the polymer chains decreases as the polymer chain within the crystal becomes more conjugated (due to planarity of the backbone) and the degree of the intrachain order decreases. The cross talk between the chains decreases as the chain becomes more planar because the excitons can delocalize more easily within the chain [14, 20-23]. It is intriguingly interesting to note that there is no outright correlation between the absorption peak ratios ($A_{0\text{-}0}/A_{0\text{-}1}$), the excitonic coupling constants (j_o) and the excitonic bandwidths (W) on the solvent polarities.

3.2.2 Photoluminescence Spectroscopy

The PL technique has been widely used to investigate the energy level of materials and to provide fundamental information on the properties of the energy levels lying within the band gap. Figure 8 shows the PL spectra associated with the three samples A, B and C using 532 nm excitation frequency. There are some small differences in integrated PL intensity, sideband intensities and line width. However, there are two obvious peaks located at 692 nm and 722 nm, corresponding to the 0–0 and 0–1 electronic transition, in all of the PL spectra at room temperature.

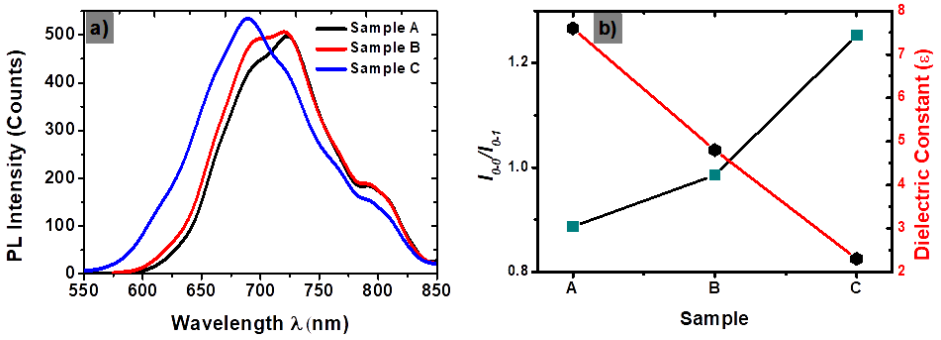

Figure 8 The PL spectra collected from sample A, B and C (a) and the graph showing increasing $I_{0\text{-}0}/I_{0\text{-}1}$ intensity ratios in PL with decreasing solvent dielectric constants

The H- and J-type excitonic coupling gives rise to different selection rules for absorption and emission. We can thus determine the nature of the coupling from qualitative differences observed in the absorption or emission spectra [14, 22]. In weakly coupled H-aggregate systems, the $I_{0\text{-}0}$ transition in emission is only weakly allowed due to structural or thermal disorder, and most of the photoluminescence (PL) intensity is carried in the 0-1 vibronic transition. This gives rise to $I_{0\text{-}0}/I_{0\text{-}1}$ intensity ratios in PL < 1 for H-aggregate systems [14, 22]. For, a rigid planar thiophene rings, there is better intrachain coupling manifested as Jaggregate behavior. The 0-0 transition in emission is strongly allowed, thus giving rise to $I_{0\text{-}0}/I_{0\text{-}1}$ intensity ratios in PL greater than 1[14, 20-26]. From our results as shown in Figure 8, there is an increase in $I_{0\text{-}0}/I_{0\text{-}1}$ intensity ratios for the decreasing dielectric constant from the samples A, B and C respectively (decreasing in solvent polarities).

In the H/J aggregate model, this observed increase in the 0-0 peaks implies that the intrachain bandwidth is now larger relative to the interchain bandwidth [14, 20-26]. Further, there is increase in

PL intensity as shown in Figure 8. This could be as a result of a relatively larger reduction in the interchain coupling from sample A to sample B to sample C (decreased solvent polarities). This is supported by the blueshift in the luminescence in that order. This is also supported by the reduction in Stokes' shifts as shown in Figure 9.

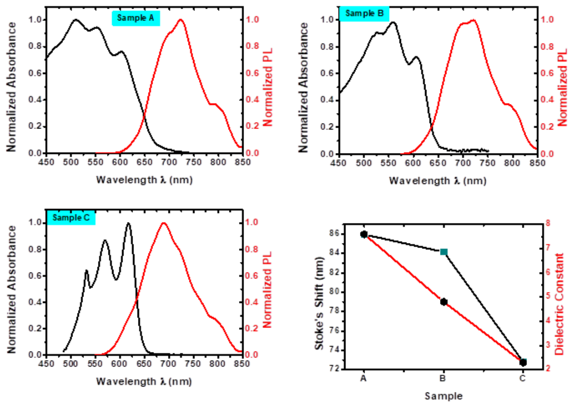

Figure 9 The absorption and the PL spectra collected from sample A, B and C showing decrease in Stoke's shift with decreasing solvent polarities

It is important to note that if the interchain coupling is reduced, then the spectral separation between the higher-energy absorbing state and the lower-energy emitting state caused by interchain coupling must also be reduced, causing a blue shift in the emitting state as the band narrows.

3.2.3 The Optical Band Gap Energy

The PL emission is normally affected by the polarity of the solvent system and shifted with change in polarity of solvent. However, the absorption spectra are comparatively much less affected by change in solvent polarity. For the aforementioned reasons, the PL emissions do not give exact band gap and so we have chosen calculating band gap. The band-gap energy E_g is associated with the HOMO to LUMO electron transitions between the π and π* molecular orbitals [14, 20-29]. Optical spectra give information about the optical excitation of an electron from the ground to the first excited state .This can be estimated using Tauc's relation;

$$\alpha h\upsilon = A(h\upsilon - E_g)^{1/2} \quad (7)$$

The relation applies to direct band-gap energy material. Here, *hυ* is the incident photon energy). The absorption coefficient, α was calculated by using Beer-Lambert's law.

$$\alpha = 2.303A/d \quad (8)$$

where, A is the absorbance and d is the thickness. The determined band gap values is obtained by extrapolating the linear region of the plot $(\alpha h\nu)^2 = 0$. The allowed direct transition optical gap is found as 2.065 eV, 1.907 eV and 1.775 eV for samples A, B and C as shown in Figure 10. These downshifts are attributed to the thiophene ring in the polymer P3HT.

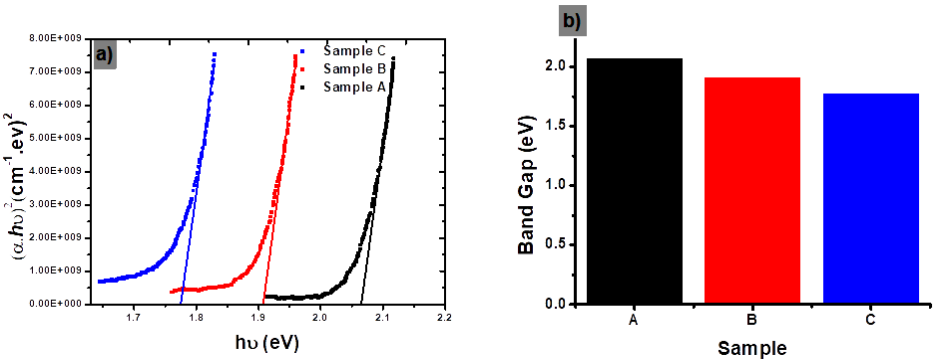

Figure 10 A graph of (α h υ)2 versus photon energy (hυ) for P3HT crystals (a) and a bar graph showing decreasing band gap energy of P3HT crystals with the solvent used for fabrication (b).

From the graphs, there are increased optical band gap energies with increased polarities of the solvents.

4. Conclusion

We have shown that the solvent quality for P3HT generally decreases with increasing polarities (dielectric constants) of the solvents. Accordingly, we have asserted that the self-assembly behavior of the polymer greatly depends on the solvent polarity rather than their solubility power. This is because as the solvent polarity increases, the interaction between P3HT and the solvent decreases and the interaction between the polymer chains become more dominant. Consecutively, P3HT chains slowly aggregate into low order crystalline structures, in which the polymer chains are randomly entangle. The solvent polarities thus have their fingerprints in the resultant film crystallinities, grain sizes, optical photoluminescence and the optical band gaps and by extension on the opto-electronic device applications.

Acknowledgements

We would like to extend our appreciation to Pwani University for availing the laboratory and necessary equipment and materials that made this research possible.

References

1. Chirvase D, Chiguvare Z, Knipper M, Parisi J, Dyakonov V, Hummelen JC. Electrical and Optical design and characterization of regioregular poly(3-hexylthiophene-2,5diyl)/ fullerene-based heterojunction polymer solar cells. ***Synthetic Metals*.** 2003, 138:299-304
2. Jeffries E, McCullough RD. Conjugated polymers theory, synthesis, properties, and characterization, in regioregular polythiophenes. *T.A.S.a.J.R. Reynolds*, ***CRC Press, Taylor & Francis Group***; 2007
3. Al-Ibrahim M, Roth H K, Schroedner M, Konkin A, Zhokhavets U, Gobsch G, Scharff P, Sensfuss, ***S. Organic Electronics*.** 2003, 6:65-71
4. Chang JF, Sun B, Breiby DW, Nielsen MM, Soelling TI, Giles M, McCulloch I, Sirringhaus H. Enhanced Mobility of Poly(3-hexylthiophene) Transistors by Spin-Coating from High-Boiling-Point Solvents. ***Chem Mater*.** 2004, 16:4772-4776
5. Osterbacka R, An CP, Jiang XM, Vardeny ZV. 2001, ***Synth Met*.** 116:317-323

6. Zhao K, Xue L, Liu J, Gao X, Wu S, Han Y, Geng Y. A new method to improve poly(3-hexyl thiophene) (P3HT) crystalline behavior: decreasing chains entanglement to promote order-disorder transformation in solution, **Langmuir.** 2010, 26:471-477
7. Chen CY, Chan SH, Li YJ, Wu KH, Chen HL, Chen JH, Huang WY, Chen SA. Formation and Thermally-Induced Disruption of Nanowhiskers in Poly(3-hexylthiophene)/Xylene Gel Studied by Small-Angle X-ray Scattering. **Macromolecules**. 2010, 43:7305-7311
8. Wu C, Wang X. Globule-to-Coil Transition of a Single Homopolymer Chain in Solution. **Phys. Rev. Lett.** 1998, 80:4092-4094.
9. Knaapila M, Garamus VM, Dias FB, Almásy L, Galbrecht F, Charas A, Morgado J, Burrows HD, Scherf U, Monkman AP. Structure and Dynamics of Nondilute Polyfluorene Solutions**. Macromolecules.** 2006, 39:6505-6512
10. Lim KC, Fincher CR. Heeger AJ. Rod-to-Coil Transition of a Conjugated Polymer in Solution. **Phys. Rev. Lett.** 1983, 50:1934-1937
11. Hu D, Yu J, Bachl B, Rossky PJ, Barbara PF. Solvent quality-induced nucleation and growth of parallelepiped nanorods in dilute poly(3-hexylthiophene) (P3HT) solution and the impact on the crystalline morphology of solution-cast thin film. **Nature**. 2000, 405**:**1030-1033
12. Gedde UW. *Polymer Physics*. New York: **Chapman & Hall**; 1995
13. Machui F, Langner S, Zhu XD, Abbott S, Brabec CJ. Determination of the P3HT:PCBM Solubility Parameters via a Binary Solvent Gradient Method: Impact of Solubility on the Photovoltaic Performance. **Solar Energy Materials & Solar Cells**. 2012, 100:138-146
14. Spano FC, Silva CH- and J-Aggregate Behavior in Polymeric Semiconductors. **Annu. Rev. Phys. Chem.** 2014, 65:477-500
15. Erb T, Gobsch G, Raleva S, Stühn B, Schilinsky P, Waldauf C, Brabec CJ. Correlation Between Structural and Optical Properties of Composite Polymer/Fullerene Films for Organic Solar Cells. **Adv. Funct. Mater.** 2005, 15**,** 1193
16. Kippelen B, Bredas J L. Organic photovoltaics. **Energy Environ. Sci.** 2009, 2:251-256
17. Grätzel M. Photoelectrochemical cells. **Nature.** 2001, 414:338-344
18. Heffner GW, Pearson DS. Molecular Characterization of. Poly(3-hexylthiophene). **Macromolecules.** 1991, 24:6295-6299
19. Zen A , Pflaum J, Hirschmann S, Zhuang W, Jaiser F, Asawapirom U, Rabe J B, Scherf U, Neher D, **Adv Funct Mater.** 2004, 14:757-764
20. Niles ET, PhD dissertation presented to Department of Chemistry, The University of New Mexico Albuquerque. New Mexico. 2013.
21. Spano FC. The Spectral Signatures of Frenkel Polarons in H- and J-Aggregates. **Acc. Chem. Res.** 2010, 43:429-439
22. Barnes MD, Baghar M. **Journal of Polymer Science Part B: Polymer Physics**.2012, 50:1121-1129
23. Niles ET, Roehling JD, Yamagata H, Wise AJ, Spano FC, Moule AJ, Grey JK. J-Aggregate Behavior in Poly-3-hexylthiophene Nanofibers. **J. Phys. Chem. Lett.** 2012, 3**:**259-263
24. Spano FC. Yamagata H. Vibronic Coupling in J-Aggregates and Beyond: A Direct Means of Determining the Exciton Coherence Length from the Photoluminescence Spectrum. **J. Phys. Chem. B.** 2011, 115:5133-5143
25. Spano FC. Modeling disorder in polymer aggregates: the optical spectroscopy of regioregular poly(3-hexylthiophene) thin films. **J. Chem. Phys.** 2005, 122:234701. Erratum. **J. Chem. Phys.** 2007,126:159901

26. Yamagata H, Spano FC. Interplay between intrachain and interchain interactions in semiconducting polymer assemblies: The HJ-aggregate model. **The Journal of Chemical Physics.** 2012, 136:184901
27. Green MA. Third generation photovoltaics: solar cells for 2020 and beyond. **Physica: E-Low-Dimensional Systems & Nanostructures.**2002, 65-70
28. Shrotriya V, Ouyang J, Tseng R. Absorption spectra modification in poly(3-hexylthiophene):methanofullerene blend thin films. **Chemical Physics Letters**. 2005, 411, 138-143
29. Ourida O, Mohammed B. Influence of the Blend Concentration of P3HT in the Performances of BHJ Solar Cells. ***Science Academy Transactions on Renewable Energy Systems Engineering and Technology (SATRESET)***. 2011:1-3